Earth and Planetary Science Letters 621 (2023) 118372

Contents lists available at ScienceDirect

Earth and Planetary Science Letters

journal homepage: www.elsevier.com/locate/epsl

The role of internal feedbacks in sustaining multi-centennial variability of the Atlantic Meridional Overturning Circulation revealed by EC-Earth3-LR simulations

Ning Cao [a,b,c], Qiong Zhang [b,c,*], Katherine Elizabeth Power [b,c], Frederik Schenk [c,d,e], Klaus Wyser [c,f], Haijun Yang [g,h]

[a] College of Ocean and Meteorology and CMA-GDOU Joint Laboratory for Marine Meteorology, Guangdong Ocean University, Zhanjiang, 524088, China
[b] Department of Physical Geography, Stockholm University, Stockholm, 10691, Sweden
[c] Bolin Centre for Climate Research, Stockholm University, Stockholm, 10691, Sweden
[d] Department of Geological Sciences, Stockholm University, Stockholm, 10691, Sweden
[e] Department of Geosciences and Geography, University of Helsinki, Helsinki, 00014, Finland
[f] Swedish Meteorological and Hydrological Institute (SMHI), Norrköping, 60176, Sweden
[g] Department of Atmospheric and Oceanic Sciences and Institute of Atmospheric Science and CMA-FDU Joint Laboratory of Marine Meteorology, Fudan University, Shanghai, 200438, China
[h] Shanghai Scientific Frontier Base for Ocean-Atmosphere Interaction Studies, Fudan University, Shanghai, 200438, China

ARTICLE INFO

Article history:
Received 15 April 2023
Received in revised form 27 July 2023
Accepted 29 August 2023
Available online xxxx
Editor: Y. Asmerom

Keywords:
multi-centennial climate variability
EC-Earth
salinity advection feedback
vertical mixing

ABSTRACT

A significant multi-centennial climate variability with a distinct peak at approximately 200 years is observed in a pre-industrial (PI) control simulation using the EC-Earth3-LR climate model. This oscillation originates predominately from the North Atlantic and displays a strong association with the Atlantic Meridional Overturning Circulation (AMOC). Our study identifies the interplay between salinity advection feedback and vertical mixing in the subpolar North Atlantic as key roles in providing the continues internal energy source to maintain this multi-centennial oscillation. The perturbation flow of mean subtropical-subpolar salinity gradients serves as positive feedback to sustain the AMOC anomaly, while the mean advection of salinity anomalies and the vertical mixing or convection acts as negative feedback, constraining the AMOC anomaly. Notably, this low-frequency variability persists even in a warmer climate with weakened AMOC, emphasizing the robustness of the salinity advection feedback mechanism.

0. Plain language summary

Understanding climate variability over timescales longer than 100 years is challenging due to limited observational data. However, both paleoclimate proxy records and climate model simulations suggest that our climate system experiences multi-centennial variability. The driving mechanisms behind these long-lasting oscillations have been difficult to identify, with previous research suggesting that salinity anomalies from the South Atlantic or the Arctic region could be responsible. However, these explanations fail to account for the continuous internal energy source that maintains such a long period of oscillation. In our study, we analyzed a 2000-years long simulation using EC-Earth3-LR climate model under PI conditions to explore the origin of the multi-centennial climate variability. Our results revealed that the salinity advection feedback in the subtropical-subpolar North Atlantic plays a crucial role in maintaining the AMOC variability at multi-centennial time scale. Under the ongoing global warming, even though the AMOC is becoming weaker, the multi-centennial oscillation continues to persist.

1. Introduction

In recent years, variability on multi-centennial time scale has been determined as an important feature of our planet's climate system. Numerous paleoclimate proxy reconstructions, including air temperature and sea surface temperature derived from marine, lake, ice core, tree ring records, have revealed the presence of low-frequency variability (Delworth and Mann, 2000; Sicre et al., 2008; Jones et al., 2009; Mann et al., 2009; Menary et al., 2012; Srokosz and Bryden, 2015; Ayache et al., 2018; Thirumalai et al., 2018). Long term climate model simulations also support these findings

* Corresponding author at: Department of Physical Geography, Stockholm University, Stockholm, 10691, Sweden.
E-mail address: qiong.zhang@natgeo.su.se (Q. Zhang).

https://doi.org/10.1016/j.epsl.2023.118372

(Vellinga and Wu, 2004; Park and Latif, 2008; Friedrich et al., 2010; Menary et al., 2012; Delworth and Zeng, 2012; Jiang et al., 2021). A recent work by Askjær et al. (2022) has provided the evidences of existence of multi-centennial variability from spectrum analysis on 120 temperature reconstructions during the Holocene and transient Holocene simulations from 9 climate models. Significant multi-centennial variability was found to be centered in the frequency band >100 to <250 years in both proxies and models.

Notably, both proxy data and model simulations exhibit more spectral density on multi-centennial variability in the Northern high latitudes, indicating potential driving mechanisms or feedbacks concentrated in this region (Askjær et al., 2022). Several modeling studies have attributed the source of this variability to fluctuations in the North Atlantic Meridional Overturning Circulation (AMOC) (Delworth and Zeng, 2012; Lapointe et al., 2020; Jiang et al., 2021; Dima et al., 2022; Meccia et al., 2022).

Climate variability recorded in the proxy data can arise from external forcing changes (e.g., solar irradiance and volcanic eruptions, see Ottera et al., 2010; Mann et al., 2021) and internal processes (e.g., ocean-atmosphere interaction, Mann et al., 2014; Zhang et al., 2019). Previous modeling studies using simple models have also shown that low-frequency oscillations in climate system can emerge from either external forcing or internal processes. External forcing is classified as forced oscillatory, where the low-frequency variability is attributed to the AMOC's response to stochastic atmospheric forcing (Griffies and Tziperman, 1995; Roebber, 1995; Tziperman and Ioannou, 2002). However, the recent Holocene transient simulations with single forcing demonstrate that none of the external forcing, such as the solar irradiance or volcanic activity, are identified as the sole driver of the multi-centennial variability (Askjær et al., 2022).

On the other hand, simple model studies have demonstrated that self-sustained oscillation can arise when the ocean generates its own oscillation, often due to local vertical density profiles or salinity advection feedback (Welander, 1982; Rivin and Tziperman, 1997; Zhang et al., 2002; Colin de Verdiere et al., 2006). Li and Yang (2022) recently introduced an enhanced mixing mechanism in the subpolar North Atlantic using a single-hemisphere 4-box model, which enables the AMOC to exhibit a self-sustained multi-centennial oscillation. This mechanism allows the 4-box model to approximate a reduced 3-box model, facilitating the theoretical solution to the multi-centennial oscillation. The oscillation period is determined by the system's eigenvalue, which is fundamentally controlled by the upper ocean's turnover time. Their study also reveals that the multi-centennial oscillation can be excited by stochastic freshwater forcing. These findings suggest that the North Atlantic Ocean has an intrinsic multi-centennial mode, which could help better understand the multi-centennial variability identified in paleoclimatic proxy data.

Several studies using control simulations employing fully coupled ocean-atmosphere model have suggested that the multi-centennial variability is driven by salinity anomalies in the North Atlantic. However, the mechanism underlying the origins of these salinity anomalies differs among these modeling studies. Some propose freshwater transport from the South Atlantic (Park and Latif, 2008; Delworth and Zeng, 2012), while others suggest atmospheric feedback in the equatorial Atlantic Ocean (Vellinga and Wu, 2004), or freshwater exchanges between the Arctic and North Atlantic regions (Jiang et al., 2021; Meccia et al., 2022). Although these studies offer partial explanations for AMOC fluctuations, they have not yet identified a continuous energy source that drives this long-lasting oscillation.

A distinct 200-year oscillation has recently been observed in our 2,000-year output from a PI control experiment using the fully coupled EC-Earth3-LR climate model. This long simulation presents a unique opportunity for a thorough diagnostic analysis of the model output to investigate the underlying mechanism. In this paper, we elucidate the physical processes that enable the multi-centennial oscillation to persist in our simulation. Our results reveal that interplay between salinity advection feedback and vertical mixing in the subtropical-subpolar North Atlantic is crucial for maintaining this multi-centennial variability, which aligns with the theory proposed by Li and Yang (2022). By examining these mechanisms from the fully coupled climate model, we aim to deepen our understanding of multi-centennial variability and contribute to the ongoing research in this area.

2. Data and methods

2.1. Model description and experimental design

EC-Earth is a fully coupled Earth system model, designed to provide an integrated view of our planet's climate. It is developed by the European consortium involving expertises from more than 30 research institutions and the model enables researchers to study a wide range of climate-related topics, including climate change simulations, predictions, sensitivity studies, and process studies (Semedo et al., 2016; Wyser et al., 2020a,b; Zhang et al., 2021; Myriokefalitakis et al., 2022).

The EC-Earth model consists of multiple components such as atmosphere, ocean, sea ice, land and biosphere, which are coupled together to simulate a detailed and complete picture of the Earth's climate system. In this study, we use the EC-Earth3-LR configuration, which couples the atmosphere, land, ocean and sea-ice components. LR stands for low resolution for the atmospheric and land model. The atmospheric component of the model is based on the Integrated Forecasting System (IFS) model with horizontal resolution of about 125 km (T159) and 62 vertical levels (L62), while the ocean component utilizes the Nucleus for the European Modelling of the Ocean version 3.6 (NEMO3.6), with horizontal resolution of about 1° (ORCA1) and 75 vertical levels (L75). NEMO also includes the Louvain-la-Neuve Sea-ice model version 3 (LIM3), a dynamic and thermodynamic sea-ice model with five ice thickness categories. For a more in-depth look at the latest model development, refer to Döscher et al. (2022).

To test the model's capabilities, we conducted a control simulation using the PI conditions. This involved initializing the model with a steady restart file, obtained from 500-year PI control simulation, and then running it for 2000 years. We also explored the model's sensitivity to the changing CO_2 level by conducting two additional experiments, which changed CO_2 concentration to 400 ppm (E400) and 560 ppm (E560) and were integrated for over 3000 years. We used the final 2000-year outputs of these simulations to investigate the multi-centennial climate variability.

2.2. Proxy data and observational data sources

To gain insights into the North Atlantic's past climate, we have selected reconstruction data from six sites featured in the "Temperature 12k Database" (Temp12k) by Kaufman et al. (2020). These data include four sites in Greenland, one in Iceland, and another in the Central and Eastern Pyrenees.

Additionally, we have utilized the Hadley Centre Central England Temperature (HadCET, Parker et al., 1992) dataset, which is the world's longest instrumental record and begins in 1659 (https://www.metoffice.gov.uk/hadobs/hadcet/). These temperatures are representative of a roughly triangular area of the United Kingdom enclosed by Lancashire, London and Bristol, and are now kept up to date by the Climate Data Monitoring section of the Hadley Centre, Met Office.

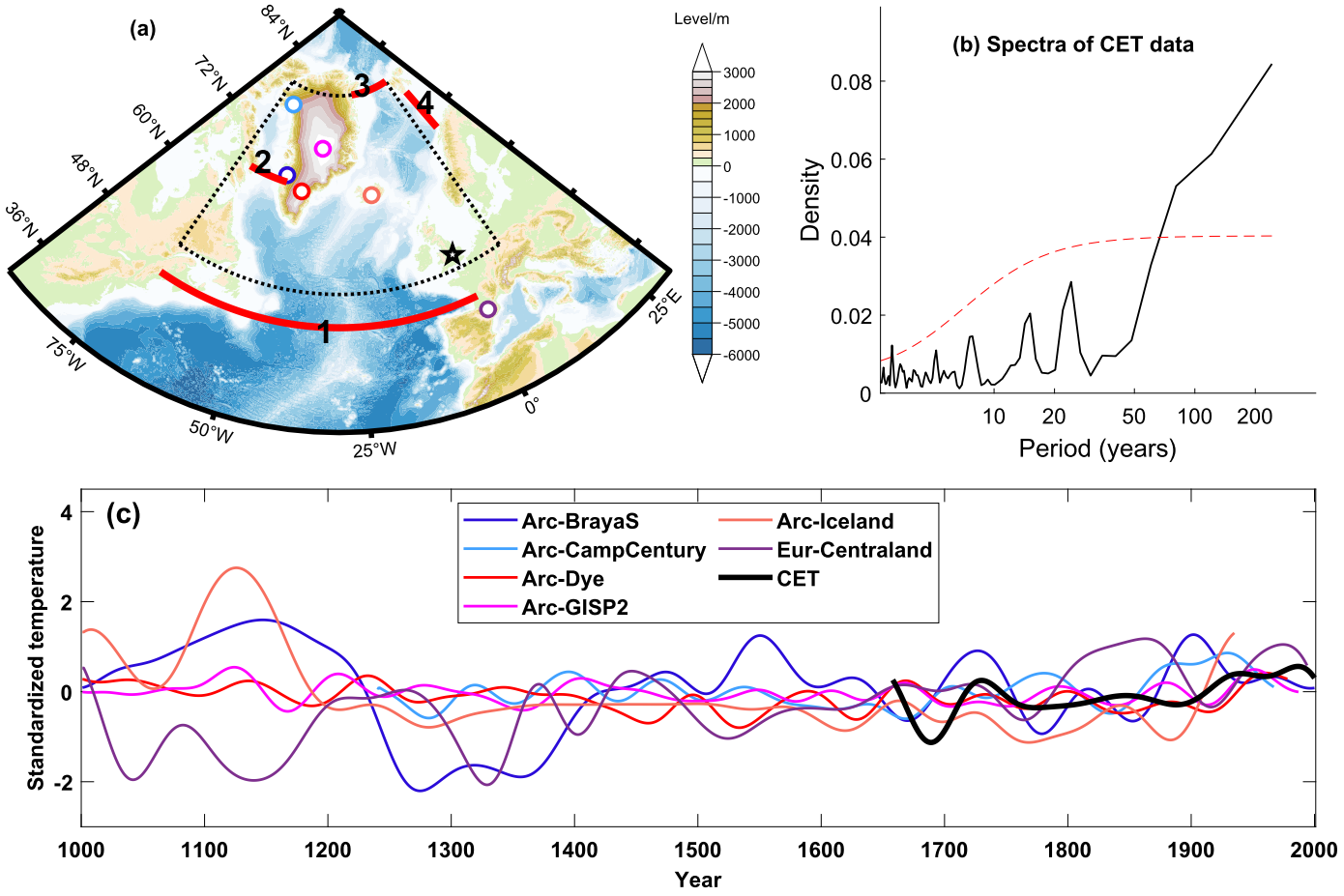

Fig. 1. (a) Locations of six proxy records (circles) and the Central England Temperature (CET) record (star) with a base map from ETOPO2, and the North Atlantic Deep-Water (NADW) formation region is marked as a dotted box, and red lines indicate the boundaries between the North Atlantic and the Arctic through the Baffin Bay (2), the Fram Strait (3) and the Barents Sea (4), while line 1 indicates the boundary between the Subpolar North Atlantic and the Subtropical North Atlantic; (b) Spectra of the longest yearly mean observed temperature for the Midlands region of England (CET record) following the red noise significant test; (c) Standardized proxy temperature records at six locations and the CET record. Proxy records are interpolated using a Modified Akima Interpolation in MATLAB. All time series are low-pass filtered with the Lanczos method, using 100 weights and a cutoff period of 60 years.

3. Presence of multi-centennial variability in the observation and model control simulation

Multi-centennial climate variability has long been a topic of interest among the climate researchers. Evidence supporting its existence can be found in proxy reconstructions, transient Holocene simulations, and control simulations using coupled climate models as mentioned in the introduction. We have previously analyzed 120 proxy records collected globally from the "Arctic Holocene Proxy Climate Database" (AHPC) by Sundqvist et al. (2014) and the "Temperature 12k Database" (Temp12k) by Kaufman et al. (2020), as detailed in Askjær et al. (2022). Building on this work, we have selected 6 proxy records from around the North Atlantic (Fig. 1a) to further explore the multi-centennial variability. Our low-pass filtered time series analysis reveals a dominant multi-centennial variability with period ranging from 100 to 250 years (Fig. 1c), confirmed the results from a large group of data in Askjær et al. (2022).

In addition, we have examined the Central England Temperature (CET), the longest instrumental temperature record available from the year 1659, as a realistic reference for low-frequency climate variability. Our spectral analysis of the unfiltered yearly mean temperature (1659-2022) from CET dataset, shown in Fig. 1b, shows a low-frequency spectrum with the most significant variance at time scales of century to multi-century years.

In our PI simulation with EC-Earth3-LR, as is shown in Fig. 2(a), the global mean near-surface air temperature time series displays significant multi-centennial variability, with standard deviation of 0.18 °C. The Northern Hemisphere exhibits even larger variations, with a standard deviation of 0.28 °C, and the Southern Hemisphere shows smaller variations with a standard deviation of 0.13 °C. Interestingly, we also examined the observed global mean temperature from 1880 to 2022 and found that it exhibits comparable fluctuations with standard deviation of 0.18 °C after removing the linear trend.

4. Searching for drivers of multi-centennial variability: AMOC versus zonal and vertical propagation of salinity anomaly

Proxy records and transient simulations used in Askjær et al. (2022) demonstrate that the multi-centennial variability is a global signal rather than a regional one. However, external forcing may trigger such low frequency signals in these datasets. In our PI control experiment, with the absence of external forcing, the multi-centennial variability can be studied as an internal variability of the climate system. The multi-centennial variability is most pronounced in the northern hemisphere in our PI simulation, particularly around the subpolar North Atlantic (see Fig. 2b), which can also be seen in transient Holocene simulations with different climate models (Askjær et al., 2022), as well as other control

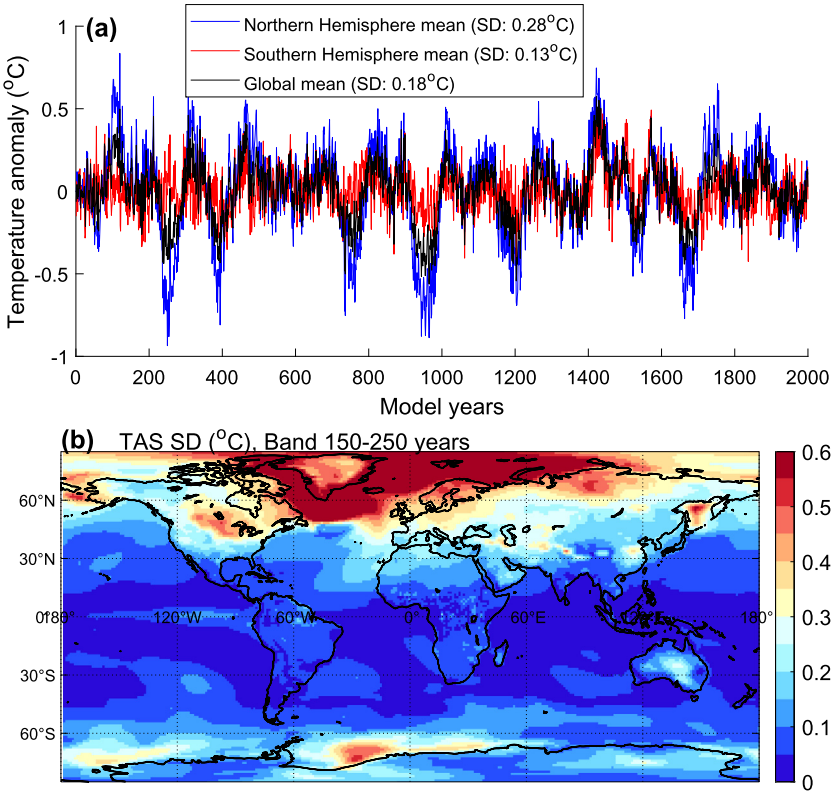

Fig. 2. (a) Time series of anomalous global mean (black), Northern Hemisphere mean (blue) and Southern Hemisphere mean (red) near-surface air temperature from the PI control simulation with the EC-Earth3-LR model. (b) Standard deviation (SD) of near-surface air temperature for 150-250 years frequency bands obtained using bandpass function in MATLAB.

simulations using different models that was reported in previous studies.

The variation of meridional ocean heat transport across 40°N in the Atlantic is highly consistent with the global mean surface air temperature (Fig. 3a,b), considered to trigger the temperature changes in the Northern Hemisphere (Delworth and Zeng, 2012). This suggests that the AMOC drives northward ocean heat transport, which is in line with the previous suggestions the AMOC mainly drives low-frequency variabilities in the Earth's climate system (Delworth and Zeng, 2012; Lapointe et al., 2020; Dima et al., 2022). We define the AMOC index as the annual-mean maximum ocean overturning stream function between 20°N to 70°N from depths 200 to 3000 meters. Fig. 3c shows the time series of the AMOC index, with an average strength of 17.5 ± 1.3 Sv (1 Sv = 10^6 m^3 s^{-1}). The variation of the AMOC is highly correlated with the global mean surface air temperature, with a correlation coefficient of 0.60.

For the variability of AMOC, two classes of oscillations have been long known and covered extensively in the 1990s: (1) damped AMOC/thermohaline oscillations driven by stochastic noise, for example, due to atmospheric weather variability, and (2) self-sustained AMOC/thermohaline oscillations. A given model can transition between these two regimes via a Hopf bifurcation, which can lead from damped to self-sustained variability as a result of a change in a friction/diffusion parameter or the strength of the mean freshwater forcing.

Previous modeling studies suggest that the AMOC variation is mainly driven by density fluctuation in North Atlantic Deep-Water (NADW) formation region (Danabasoglu, 2008; Delworth and Zeng, 2012; Dima et al., 2022). Our simulation supports this viewpoint (see Figures S1 & S2 in the supplement material). Seawater density is influenced by temperature and salinity, with salinity variation dominating overall density fluctuation in the NADW regions. Following the work of Delworth and Zeng (2012), the NADW formation region is defined as the horizontal ocean area between 70°W - 10°E and 50°N - 80°N, encompassing the Labrador Sea, Irminger Sea, and Greenland-Icelandic-Norwegian (GIN) Seas, collectively referred to as the subpolar North Atlantic in this work, as is shown in Fig. 1a. Our simulation shows that sea surface temperature (SST, Fig. 3d) and sea surface salinity (SSS, Fig. 3e) averaged over the subpolar area exhibit variations quite similar to those of the AMOC index, with correlation coefficients of 0.69 (SST) and 0.61 (SSS) respectively. Spectrum analyses of these time series reveal comparable spectra with a distinct peak around 200 years (Fig. 3f).

4.1. AMOC versus zonal advection of salinity anomalies

To explore the origin of salinity anomalies in the subpolar area, Fig. 4 presents the Hovmöller diagrams of the regressed zonal-integral salinity, averaged at ocean layers of 0-100, 100-300, 300-500, 500-1000, 1000-2000 and 2000-3000 m across the Atlantic and Arctic basins, onto the low-pass-filtered AMOC time series. At the surface layer (0-100 m, Fig. 4a), salinity anomalies are most pronounced in the subpolar area, with no significant salinity anomalies originating from the South Atlantic to the mid-latitude Atlantic, unlike that in Delworth and Zeng (2012). At the subsurface layer (100-300 m, Fig. 4b), anomalies in the subpolar area are weaker than those in the surface layer, and a stable connection between the subpolar and subtropical regions forms roughly within 100 years. Anomalies in the subtropical region strengthen at the 300-500 m layer (Fig. 4c). At depth greater than 500 m (Fig. 4d∼f), a clear southward advection of lagged salinity anomalies appears, resulting from strong convection in the subpolar area and the related southward flow to the lower AMOC branch. The upper layer salinity anomalies in the subpolar area are locally driven, possibly associated with local salinity change in the subpolar Atlantic.

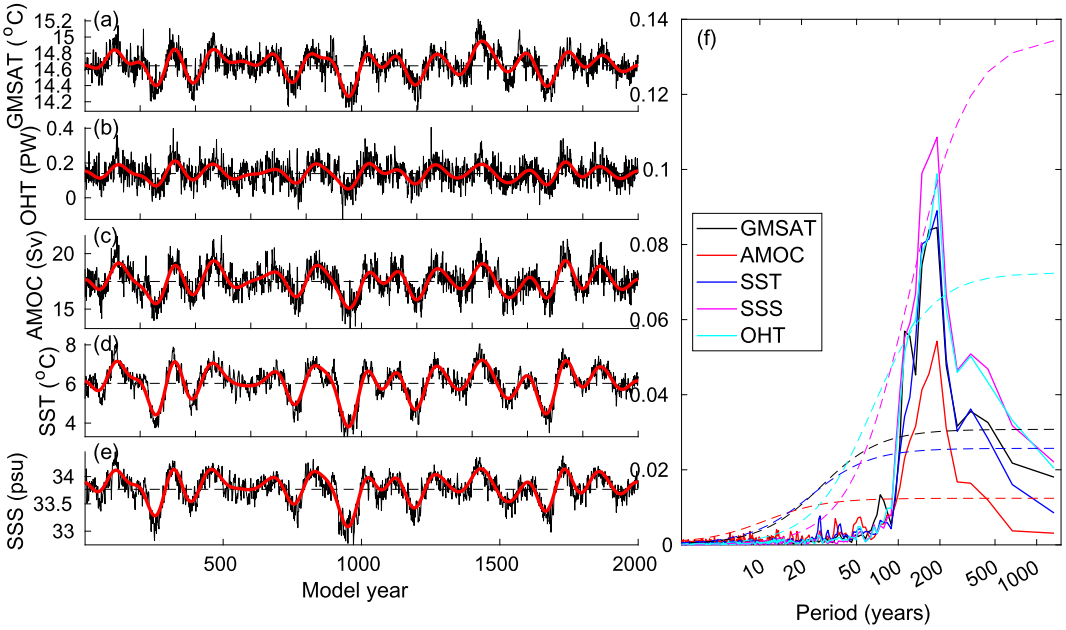

Fig. 3. (a∼e) Time series of global mean surface air temperature (GMSAT), ocean heat transport crossing 40°N in the Atlantic (OHT, 1 PW = 10^{15} Watt), AMOC index, sea surface temperature (SST) and sea surface salinity (SSS) averaged over the subpolar area, along with the low-pass filtered series (red curves, using Lanczos method with 201 weights and a 100-year cutoff period); (f) Power spectra of these corresponding time series.

The accumulated anomalies at the upper layer subpolar North Atlantic can sink and propagate southward with the help of the mean AMOC, reaching depth of up to 3000 m in the North Atlantic (Fig. 4f).

Besides, the salinity anomalies in the Arctic are also apparent in the upper 300 m ocean layer, as shown in Fig. 4a&b. It seems that a clear southward propagation from the Arctic (north of 80°N) to the North Atlantic, which was considered as the key driver of multi-centennial variability of AMOC (Jiang et al., 2021; Meccia et al., 2022). They suggested that when AMOC resides in its strong phase, the Arctic Ocean is warmed, and thus more sea-ice melting and southward freshwater transport will hamper the deep convection and driving AMOC into its negative phase. There indeed are coherent relations between the subpolar North Atlantic and the Arctic in our results. However, the Arctic Ocean is relatively a separate ocean basin, which connects with the Atlantic through the Fram Strait, the Baffin Bay and the Barents Sea. Thus the transports through these boundaries are quite limited. In Fig. 1a, the NADW formation region is marked as a dotted box, and red lines indicate the boundaries between the North Atlantic and the Arctic through the Baffin Bay (2), the Fram Strait (3) and the Barents Sea (4), while line 1 indicates the boundary between the Subpolar North Atlantic and the Subtropical North Atlantic. The salinity transports across four boundaries are computed, and the results are shown in Figure S3 in the supplement material. The mean salinity transport from the subtropical North Atlantic to the subpolar North Atlantic in the upper 1000 m layer across boundary 1 is 406.53 ± 71.17 psu·Sv (mean value ± a standard deviation), while that from the Arctic to the subpolar North Atlantic across boundaries 2, 3 & 4 is 49.74 ± 22.87 psu·Sv. On average, the salinity transports from the Arctic to the Atlantic are quite limited, through boundaries 2, 3, 4, with less than 50 psu·Sv. Meanwhile, the salinity transport through boundary 1 shows a mean value larger than 400 psu·Sv, which is about 8 times larger than that from the Arctic. For the variations, transport across boundary 1 also shows more than 3 times stronger than that of transport from the Arctic. This confirms the dominant and driving role of salinity transport from the subtropical basin in the AMOC change, which in turn drives the multi-centennial oscillation in the Arctic oceans. The multi-centennial salinity variation in the subpolar North Atlantic is dominated by processes related to large-scale circulation in the subtropical-subpolar basin.

Surface freshwater fluxes including precipitation, evaporation and condensation, liquid water runoff and solid masses that enter the ocean from land-ocean boundaries, and the melt or freezing of sea ice, being represented with the virtual salt flux at the ocean surface, is also computed. Results show that the freshwater flux at the ocean surface result an overall virtual salt flux of 8.17 ± 0.95 psu·Sv and its role in the AMOC variation can be neglected. Thus, the following analysis will focus on the salinity advection feedback and vertical mixing in the North Atlantic.

4.2. AMOC versus vertical mixing of salinity anomalies

Fig. 5 displays the latitude-depth profiles of zonally integrated salinity across the Atlantic and Arctic basins, regressed on the AMOC time series at interval of 20 years, covering a range from 80 years prior to the AMOC maximum to 100 years after it. The salinity variability follows a cycle of approximately 200 years, in line with Fig. 3f.

From 80 to 60 years prior to the AMOC maximum, negative salinity anomalies span the entire subpolar North Atlantic from surface to deep ocean, most pronounced in the upper-500 m layer. Positive anomalies are observed in the subsurface layer of the subtropical North Atlantic. The negative anomalies in the subpolar region descend deeper, reducing surface anomalies, while positive anomalies in the subtropical area intensify and expand.

At 40 years before the AMOC maximum, the subpolar upper layer anomalies transition from negative to positive, while negative anomalies in the deep ocean shift southward. Subsequently, the positive anomalies in the subpolar area grow rapidly, and negative anomalies occupy the subtropical North Atlantic deep ocean.

When the AMOC reaches its maximum (lag 0), positive salinity anomalies fill the entire subpolar area, with noticeable vertical mixing around 60°N. The negative anomalies in the subtropical lower ocean rise with enhanced amplitudes and connect with the negative salinity anomalies around 10°N at a depth of roughly 300 m.

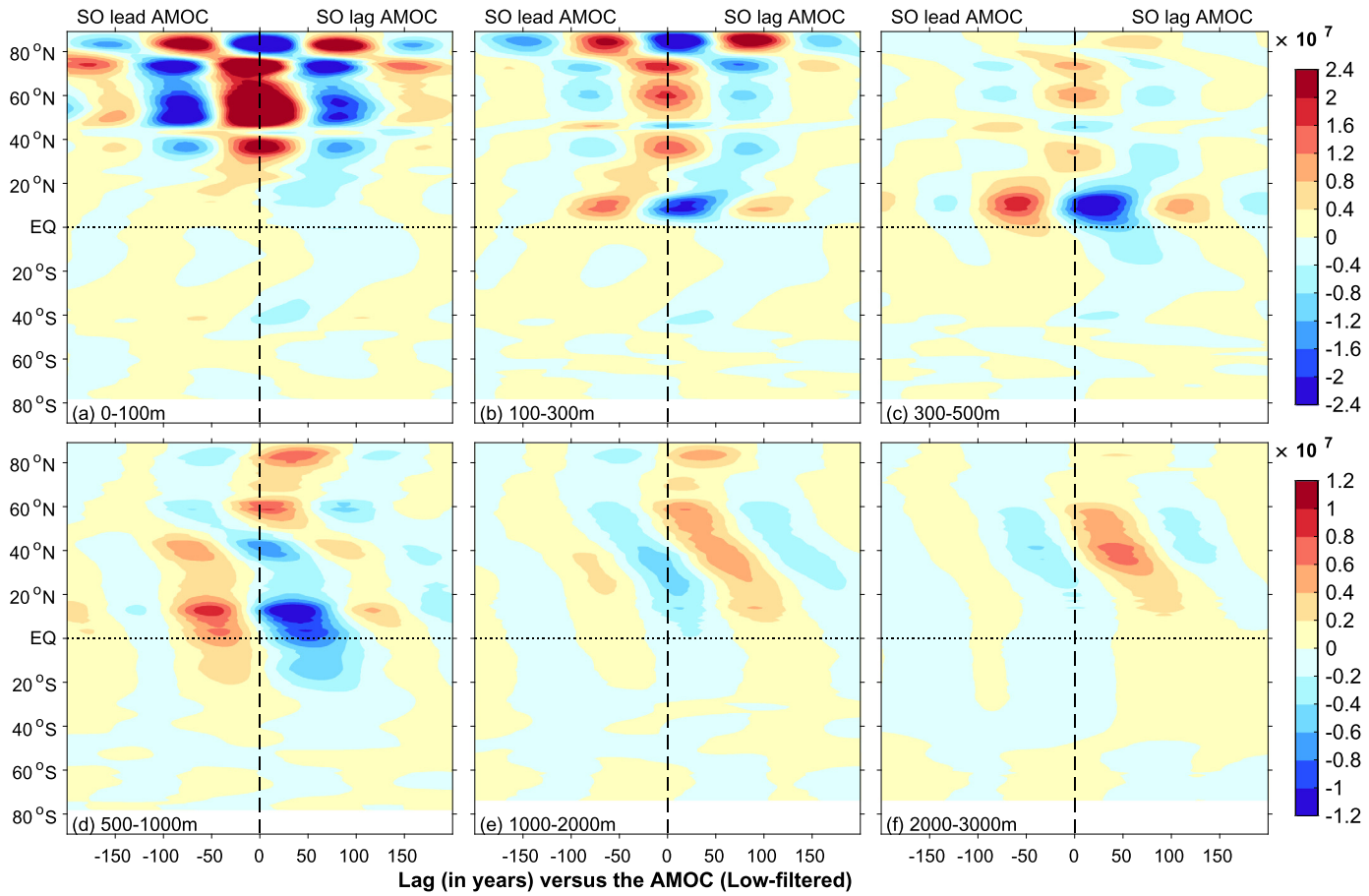

Fig. 4. Zonal integral of salinity regression coefficients across the Atlantic basin versus the low-pass-filtered AMOC time series. Units are psu m Sv^{-1}. The y-axis represents latitude, and the x-axis represents lag time of maximum AMOC. Negative (positive) values on the time axis indicate periods leading (lagging) to the maximum AMOC. (a-f) Mean values at layers of 0-100, 100-300, 300-500, 500-1000, 1000-2000, and 2000-3000 m, respectively.

Over the next 40 years, positive anomalies in the subpolar region sink into the deep ocean, weakening the surface anomalies. The negative anomalies in the subtropical region strengthen, and by lag 40, most subpolar positive anomalies have sunk into the deep ocean, moving southward. The negative anomalies in the subtropical region continue to intensify and expand.

At lag 60, the subpolar upper layer salinity anomalies shift from positive to negative, and the sinking positive anomalies in the deep ocean continue southward. Negative anomalies in the upper subpolar ocean and positive anomalies in the subsurface layer both strengthen.

By lag 100, the subpolar area displays a clear descent of negative anomalies, with a pattern similar to lag −80, signifying the beginning of a new oscillation cycle.

Figs. 4 and 5 demonstrate that surface salinity anomalies in the subpolar North Atlantic mainly originate locally rather than being transported from lower latitudes or the Arctic. We discover that these local salinity anomalies (Fig. 4a-b) result from perturbation advection of mean salinity. In contrast, deeper ocean salinity changes (Figs. 4e-f) are attributed to mean advection of salinity anomalies. Perturbation salinity advection acts as positive feedback, amplifying the local signal in the upper ocean (Fig. 4a-b). Meanwhile, mean salinity advection acts as negative feedback, generating a southward-propagating signal in the lower ocean (Figs. 4e-f) and removing the anomalies from the subpolar North Atlantic.

4.3. The role of salinity advection feedback and vertical mixing in the subpolar North Atlantic in sustaining the AMOC oscillation

Our above findings from the coupled climate model simulation align with the theory of Li and Yang (2022), which states that the perturbation salinity feedback provides the energy source for maintaining the oscillation, while mean salinity feedback dampens the salinity anomalies. In their theory, enhanced mixing in the subpolar ocean is also considered as a critical mechanism for weakening the positive salinity advection feedback and limiting oscillation amplitude. This vertical mixing of salinity anomalies can be clearly seen in Fig. 5 at the subpolar North Atlantic latitudes.

To estimate these effects, we used small-perturbation theory on the salinity equation, ignoring the nonlinear advection terms. We divided anomalous meridional salinity advection into perturbation advection of mean salinity gradients and mean advection of salinity anomaly. We defined four boxes in the North Atlantic (shown in Fig. 5 on vertical profile view): Box-1 represents the subtropical upper layer (0 - 40°N, 0-300 meters deep); Box-2 represents the subpolar upper layer from (50 - 80°N, 0-300 meters deep, between 70°W to 10°E); Box-3 represents the subpolar deep layer (50 - 80°N, 1000-3000 meters deep, between 70°W to 10°E); and Box-4 represents the subtropical deep layer (0 - 40°N, 1000-3000 meters deep).

Seawater salinity variations in Box-2 can be determined by an equation suggested in Li and Yang (2022) (Eq. 8a).

$$V_2\dot{S}_2 = q'\left(\overline{S_1} - \overline{S_2}\right) + \overline{q}\left(S_1' - S_2'\right) - k_m(S_2' - S_3') \quad (1)$$

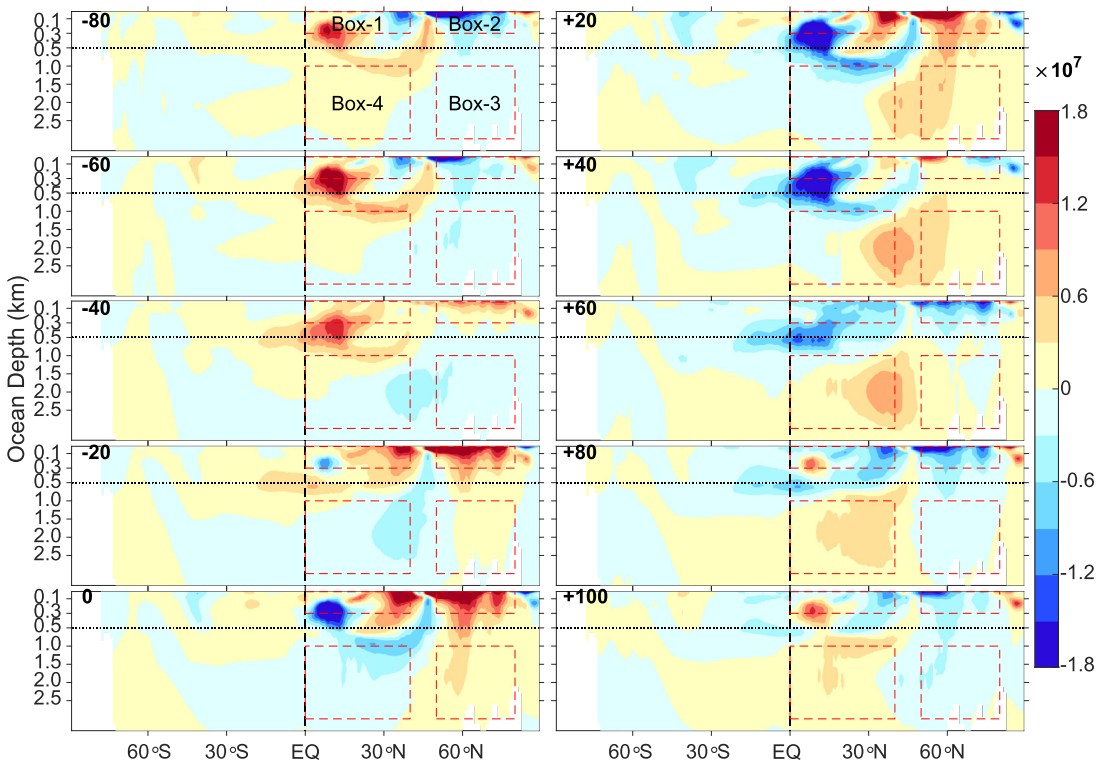

Fig. 5. Latitude-depth profiles of zonal integral salinity across the Atlantic and Arctic basins, regressed on the 100-year low-pass filtered AMOC time series. The lag is positive when the AMOC leads. Units are psu m Sv^{-1}. The scale of layers shallower than 500 m is amplified by two.

where V_2 is the volume of Box-2, q is the volume transport by the AMOC which can be divided into a mean state $\overline{q}$ and a perturbation q', S_i' is the perturbation salinity of each ocean box, $\overline{S}_i$ is the mean salinity during the reference period. Following Li and Yang (2022), we similarly define an enhanced mixing effect coefficient $k_m = \kappa \left(q'\right)^2$, in which $\kappa = 1.0\ \mathrm{m}^{-3}$ s (note that the value of κ only affects the amplitude of the oscillation but not the periodicity).

Fig. 6 shows the lead-lag regression of terms contributing to salinity anomaly in Box-2 (S_2'). The perturbation flow of mean salinity gradients from Box-1 to Box-2 (black curve) coincides with the salinity anomaly, indicating positive feedback. Conversely, mean advection of salinity anomalies (red curve) counteracts the salinity anomaly, demonstrating a significant negative impact on salinity change and causing the oscillation to change phase. Vertical mixing between Box-2 and Box-3 (blue curve) also acts as negative feedback, limiting the salinity anomaly. The most noticeable southward flow related to the lower branch of the AMOC lags behind the maximum AMOC by about 40-50 years, serving as lagged indirect negative feedback (cyan curve), which helps to limit the salinity anomaly by transferring mixed anomalies from Box-3 to Box-4.

These results demonstrate that the multi-centennial variability of AMOC in our model is sustained by positive feedback from perturbation advection of mean salinity gradients, the negative feedback from mean advection of salinity anomalies, and enhanced vertical mixing in the subpolar ocean. These findings are consistent with the theoretical prediction of Li and Yang (2022).

5. Conclusion and discussion

In a 2000-year PI control simulation using the EC-Earth3-LR climate model, we identified significant multi-centennial variability with a timescale of approximately 200 years in global mean surface air temperature. This variability can be attributed to AMOC fluctuations. A strengthened AMOC correlates with positive density anomalies in the North Atlantic deep-water formation region, where salinity variations primarily drive overall density fluctuations in the subpolar area.

The mechanism maintaining multi-centennial variability in the simulated climate system is revealed in this study. Perturbation advection of mean subtropics-subpolar salinity gradients generates positive feedback for the growth of the AMOC anomalies. Meanwhile, mean advection of salinity anomalies and vertical mixing or convection serve as negative feedback, constraining AMOC anomalies. Both our fully coupled model simulation and simple conceptual model in Li and Yang (2022) suggest that subpolar salinity anomalies are mainly driven by perturbed ocean circulation on multi-centennial timescales, rather than by the mean flow of salinity anomaly from the south Atlantic (Delworth and Zeng, 2012) or the Arctic (Jiang et al., 2021; Meccia et al., 2022). The salinity advection feedback mechanism is crucial for explaining the self-sustained AMOC oscillation.

Freshwater anomalies from the Arctic do impact seawater density in the subpolar area, but they cannot be considered the primary energy source for AMOC fluctuations. In Figure S4 in the supplement material, salinity and ocean current patterns in the upper 100 m ocean layer show that the anomalies in the Arctic feature opposite sign to that in the subpolar North Atlantic. But the anomalies in the subpolar North Atlantic are much stronger. Freshwater in the Arctic transporting to the subpolar North Atlantic, which is considered as the driver of seawater density fluctuations in this region in Jiang et al. (2021) and Meccia et al. (2022), cannot excite such strong anomalies without the salinity advection feedback shown in this work. The anomaly in the Arctic act as more like a response to stronger or weaker AMOC, rather than a sole driver of AMOC variations.

In a warmer climate, such as during ongoing global warming, the AMOC weakens compared to the PI period (Rahmstorf et al., 2015; Caesar et al., 2021). However, there is ongoing debate re-

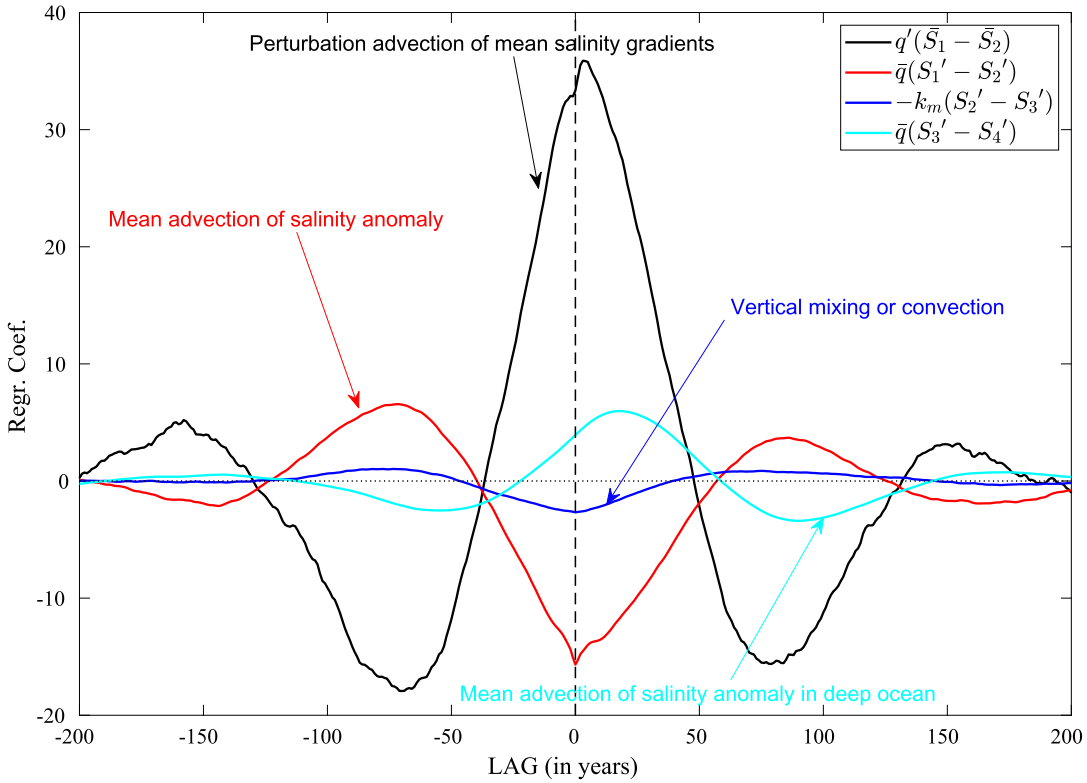

Fig. 6. Regression of three direct terms (black, red and blue curves) contributing to seawater salinity variations in Box-2 (defined in Eq. (1)), and one indirect term (cyan curve) indicating the southward flow related to the lower branch of the AMOC, onto the time series of salinity in Box-2.

garding the role of climate change versus the circulation's century-to-millennial-scale variability (Kilbourne et al., 2022; Latif et al., 2022). Our simulations under 400 ppm and 560 ppm CO_2 forcing show a weakened AMOC (Figure S5a∼c). Nevertheless, the spectra still reveal multi-centennial variability with dominant oscillation periods of around 100-300 years, as illustrated in Figure S5d. Although the oscillation amplitude is suppressed under higher CO_2 forcing, the multi-centennial scale variability of the AMOC still persists. Under 400 ppm CO_2 forcing, the spectra peaks at about 148 years, while it peaks at 256 years under 560 ppm CO_2 forcing. The total Arctic sea-ice mass under 280, 400 and 560 ppm CO_2 forcing shows that, under PI (280 ppm) simulation, the Arctic sea ice mass is $24.17 \pm 3.71 \times 10^{25}$ kg, and it is $6.61 \pm 0.97 \times 10^{25}$ kg under 400 ppm CO_2 forcing, and $2.43 \pm 0.44 \times 10^{25}$ kg under 560 ppm CO_2 forcing. This further confirms that the multi-centennial oscillation of the AMOC is an intrinsic mode in the system rather than climate state-dependent as suggested in Meccia et al. (2022). A warmer climate has the potential to suppress the oscillation amplitude and modify the oscillation periods through increased ocean heat content, enhanced freshwater flows from the melting of Greenland ice sheets and the Arctic sea-ice. The actual physical processes in these changing aspects warrant further investigation.

Our experiment has a few notable limitations. Firstly, while modern observations and many model simulations typically show decadal or multi-decadal climate variability around the North Atlantic, our PI simulation lacks this feature (although it is present in our E400 and E560 experiments, see Figure S5d). Further investigation is needed to determine the reason behind this discrepancy. It is worth mentioning that our study specifically focuses on multi-centennial variability driven by deep ocean dynamics, whereas multi-decadal variability is likely influenced by regional air-sea interactions. Secondly, the EC-Earth model is not coupled with an ice-sheet model and the Greenland ice sheet remains constant during the simulation. This might affect the freshwater fluxes in the subpolar North Atlantic. Lastly, the EC-Earth model exhibits overestimated biases in sea ice coverage over the Arctic and subpolar North Atlantic, with modeled sea ice extending too far into the Labrador Sea (Döscher et al., 2022). Consequently, it is crucial to evaluate and quantify the potential impact on these biases on the simulated multi-centennial variability in this region.

CRediT authorship contribution statement

Ning Cao: Conceptualization, Formal analysis, Investigation, Methodology, Validation, Visualization, Writing – original draft, Writing – review & editing. **Qiong Zhang:** Conceptualization, Data curation, Funding acquisition, Investigation, Methodology, Project administration, Resources, Supervision, Writing – review & editing. **Katherine Elizabeth Power:** Data curation, Validation, Writing – review & editing. **Frederik Schenk:** Writing – review & editing. **Klaus Wyser:** Validation, Writing – review & editing. **Haijun Yang:** Conceptualization, Supervision, Writing – review & editing.

Declaration of competing interest

The authors declare that they have no known competing financial interests or personal relationships that could have appeared to influence the work reported in this paper.

Data availability

The model simulated data to produce the main figures in this paper can be found at: https://doi.org/10.5281/zenodo.7304486 (a dataset of Zhang et al., 2022). Additional model output raw data are available from the corresponding authors on reasonable request.

Acknowledgements

This research was supported by the Swedish Research Council (Vetenskapsrådet, grant no. 2022-03129 and 2017-04232). Ning Cao is supported by the National Natural Science Foundation of China (72293604, 42130605, and 42075036), the program for scientific research start-up funds of Guangdong Ocean University (R17056), and the State Scholarship Fund of China Scholarship Council (201908440188). Ning Cao is also supported by the International Meteorological Institute in Stockholm (IMI) as a guest researcher. Haijun Yang is supported by the National Natural Science Foundation of China (42230403). Frederik Schenk is funded by the Swedish Research Council for Sustainable Development (FORMAS 2020-01000). The simulations with EC-Earth3-LR and data analysis were performed using the ECMWF's computing and archive facilities and Swedish National Infrastructure for Computing (SNIC) at the National Supercomputer Centre (NSC), partially funded by the Swedish Research Council through grant agreement no. 2018-05973. We extend our sincere thanks to the anonymous reviewers for their valuable constructive comments and suggestions, which have improved the quality of the manuscript.

Appendix A. Supplementary material

Supplementary material related to this article can be found online at https://doi.org/10.1016/j.epsl.2023.118372.

References

Askjær, T.G., Zhang, Q., Schenk, F., et al., 2022. Multi-centennial Holocene climate variability in proxy records and transient model simulations. Quat. Sci. Rev. 296, 107801. https://doi.org/10.1016/j.quascirev.2022.107801.

Ayache, M., Swingedouw, D., Mary, Y., et al., 2018. Multi-centennial variability of the AMOC over the Holocene: a new reconstruction based on multiple proxy-derived SST records. Glob. Planet. Change 170, 172–189. https://doi.org/10.1016/j.gloplacha.2018.08.016.

Caesar, L., McCarthy, G.D., Thornalley, D.J.R., et al., 2021. Current Atlantic Meridional Overturning Circulation weakest in last millennium. Nat. Geosci. 14, 118–120. https://doi.org/10.1038/s41561-021-00699-z.

Colin de Verdiere, A., Jelloul, M.B., Sévellec, F., 2006. Bifurcation structure of thermohaline millennial oscillations. J. Climate 19, 5777–5795. https://doi.org/10.1175/JCLI3950.1.

Danabasoglu, G., 2008. On multidecadal variability of the Atlantic meridional overturning circulation in the Community Climate System Model Version 3. J. Climate 21, 5524–5544. https://doi.org/10.1175/2008JCLI2019.1.

Delworth, T.L., Mann, M.E., 2000. Observed and simulated multidecadal variability in the Northern Hemisphere. Clim. Dyn. 16, 661–676. https://doi.org/10.1007/s003820000075.

Delworth, T.L., Zeng, F., 2012. Multicentennial variability of the Atlantic meridional overturning circulation and its climatic influence in a 4000-year simulation of the GFDL CM2.1 climate model. Geophys. Res. Lett. 39 (13), L13702. https://doi.org/10.1029/2012GL052107.

Dima, M., Lohmann, G., Ionita, M., et al., 2022. AMOC modes linked with distinct North Atlantic deep water formation sites. Clim. Dyn. 59, 837–849. https://doi.org/10.1007/s00382-022-06156-w.

Döscher, R., Acosta, M., Alessandri, A., et al., 2022. The EC-Earth3 Earth system model for the coupled model intercomparison project 6. Geosci. Model Dev. 15, 2973–3020. https://doi.org/10.5194/gmd-15-2973-2022.

Friedrich, T., Timmermann, A., Menviel, L., et al., 2010. The mechanism behind internally generated centennial-to-millennial scale climate variability in an earth system model of intermediate complexity. Geosci. Model Dev. 3, 377–389. https://doi.org/10.5194/gmd-3-377-2010.

Griffies, S.M., Tziperman, E., 1995. A linear thermohaline oscillator driven by stochastic atmospheric forcing. J. Climate 8, 2440–2453. https://doi.org/10.1175/1520-0442(1995)008<2440:ALTODB>2.0.CO;2.

Jiang, W., Gastineau, G., Codron, F., 2021. Multicentennial variability driven by salinity exchanges between the Atlantic and the Arctic Ocean in a coupled climate model. J. Adv. Model. Earth Syst. 13 (3), e2020MS002366. https://doi.org/10.1029/2020MS002366.

Jones, P.D., Briffa, K.R., Osborn, T.J., et al., 2009. High-resolution palaeoclimatology of the last millennium: a review of current status and future prospects. Holocene 19 (1), 3–49. https://doi.org/10.1177/0959683608098952.

Kaufman, D., McKay, N., Routson, C., et al., 2020. A global database of Holocene paleotemperature records. Sci. Data 7, 115. https://doi.org/10.1038/s41597-020-0445-3.

Kilbourne, K.H., Wanamaker, A.D., Moffa-Sanchez, P., et al., 2022. Atlantic circulation change still uncertain. Nat. Geosci. 15, 165–167. https://doi.org/10.1038/s41561-022-00896-4.

Lapointe, F., Bradley, R.S., Francus, P., et al., 2020. Annually resolved Atlantic sea surface temperature variability over the past 2900y. Proc. Natl. Acad. Sci. USA 117 (44), 27171–27178. https://doi.org/10.1073/pnas.2014166117.

Latif, M., Sun, J., Visbeck, M., et al., 2022. Natural variability has dominated Atlantic Meridional Overturning Circulation since 1900. Nat. Clim. Change 12, 455–460. https://doi.org/10.1038/s41558-022-01342-4.

Li, Y., Yang, H., 2022. A theory for self-sustained multi-centennial oscillation of the Atlantic meridional overturning circulation. J. Climate 35 (18), 5883–5896. https://doi.org/10.1175/JCLI-D-21-0685.1.

Mann, M.E., Zhang, Z., Rutherford, S., et al., 2009. Global signatures and dynamical origins of the little ice age and medieval climate anomaly. Science 326 (5957), 1256–1260. https://doi.org/10.1126/science.1177303.

Mann, M.E., Steinman, B.A., Miller, S.K., 2014. On forced temperature changes, internal variability and the AMO. Geophys. Res. Lett. 41 (9), 3211–3219. https://doi.org/10.1002/2014GL059233.

Mann, M.E., Steinman, B.A., Brouillette, D.J., et al., 2021. Multidecadal climate oscillations during the past millennium driven by volcanic forcing. Science 371 (6533), 1014–1019. https://doi.org/10.1126/science.abc5810.

Meccia, V.L., Fuentes-Franco, R., Davini, P., et al., 2022. Internal multi-centennial variability of the Atlantic Meridional Overturning Circulation simulated by EC-Earth3. Clim. Dyn. https://doi.org/10.1007/s00382-022-06534-4.

Menary, M.B., Park, W., Lohmann, K., et al., 2012. A multimodel comparison of centennial Atlantic meridional overturning circulation variability. Clim. Dyn. 38, 2377–2388. https://doi.org/10.1007/s00382-011-1172-4.

Myriokefalitakis, S., Bergas-Massó, E., Gonçalves-Ageitos, M., et al., 2022. Multiphase processes in the EC-Earth model and their relevance to the atmospheric oxalate, sulfate, and iron cycles. Geosci. Model Dev. 15 (7), 3079–3120. https://doi.org/10.5194/gmd-15-3079-2022.

Ottera, O.H., Bentsen, M., Drange, H., et al., 2010. External forcing as a metronome for Atlantic multidecadal variability. Nat. Geosci. 3, 688–694. https://doi.org/10.1038/ngeo955.

Park, W., Latif, M., 2008. Multidecadal and multicentennial variability of the meridional overturning circulation. Geophys. Res. Lett. 35 (22), L22703. https://doi.org/10.1029/2008GL035779.

Parker, D.E., Legg, T.P., Folland, C.K., 1992. A new daily central England temperature series, 1772-1991. Int. J. Climatol. 12, 317–342. https://doi.org/10.1002/joc.3370120402.

Rahmstorf, S., Box, J.E., Feulner, G., et al., 2015. Exceptional twentieth-century slowdown in Atlantic Ocean overturning circulation. Nat. Clim. Change 5 (5), 475–480. https://doi.org/10.1038/nclimate2554.

Rivin, I., Tziperman, E., 1997. Linear versus self-sustained interdecadal thermohaline variability in a coupled box model. J. Phys. Oceanogr. 27, 1216–1232. https://doi.org/10.1175/1520-0485(1997)027,1216:LVSSIT.2.0.CO;2.

Roebber, P.J., 1995. Climate variability in a low-order coupled atmosphere–ocean model. Tellus 47A, 473–494. https://doi.org/10.3402/tellusa.v47i4.11534.

Semedo, A., Soares, P.M., Lima, D.C., et al., 2016. The impact of climate change on the global coastal low-level wind jets: EC-EARTH simulations. Glob. Planet. Change 137, 88–106. https://doi.org/10.1016/j.gloplacha.2015.12.012.

Sicre, M.A., Ezat, U., Guimbaut, E., et al., 2008. A 4500-year reconstruction of sea surface temperature variability at decadal time-scales off North Iceland. Quat. Sci. Rev. 27 (21–22), 2041–2047. https://doi.org/10.1016/j.quascirev.2008.08.009.

Srokosz, M.A., Bryden, H.L., 2015. Observing the Atlantic Meridional Overturning Circulation yields a decade of inevitable surprises. Science 348 (6241), 1255575. https://doi.org/10.1126/science.1255575.

Sundqvist, H.S., Kaufman, D.S., McKay, N.P., et al., 2014. Arctic Holocene proxy climate database – new approaches to assessing geochronological accuracy and encoding climate variables. Clim. Past 10, 1605–1631. https://doi.org/10.5194/cp-10-1605-2014.

Thirumalai, K., Quinn, T.M., Okumura, Y., et al., 2018. Pronounced centennial-scale Atlantic Ocean climate variability correlated with Western Hemisphere hydroclimate. Nat. Commun. 9, 392. https://doi.org/10.1038/s41467-018-02846-4.

Tziperman, E., Ioannou, P., 2002. Transient growth and optimal excitation of thermohaline variability. J. Phys. Oceanogr. 32, 3427–3435. https://doi.org/10.1175/1520-0485(2002)032,3427:TGAOEO.2.0.CO;2.

Vellinga, M., Wu, P., 2004. Low-latitude freshwater influence on centennial variability of the Atlantic thermohaline circulation. J. Climate 17 (23), 4498–4511. https://doi.org/10.1175/3219.1.

Welander, P., 1982. A simple heat-salt oscillator. Dyn. Atmos. Ocean. 6, 233–242. https://doi.org/10.1016/0377-0265(82)90030-6.

Wyser, K., Kjellström, E., Koenigk, T., et al., 2020a. Warmer climate projections in EC-Earth3-Veg: the role of changes in the greenhouse gas concentrations from CMIP5 to CMIP6. Environ. Res. Lett. 15 (5), 054020. https://doi.org/10.1088/1748-9326/ab81c2.

Wyser, K., van Noije, T., Yang, S., et al., 2020b. On the increased climate sensitivity in the EC-Earth model from CMIP5 to CMIP6. Geosci. Model Dev. 13 (8), 3465–3474. https://doi.org/10.5194/gmd-13-3465-2020.

Zhang, Q., Berntell, E., Li, Q., et al., 2021. Understanding the variability of the rainfall dipole in West Africa using the EC-Earth last millennium simulation. Clim. Dyn. 57 (1), 93–107. https://doi.org/10.1007/s00382-021-05696-x.

Zhang, Q., Cao, N., Power, K.E., 2022. Simulations for pre-industrial climate using EC-Earth3-LR model — selected data for a study on AMOC (Version 2) [Data set]. Zenodo. https://doi.org/10.5281/zenodo.7304486.

Zhang, R., Follows, M., Marshall, J., 2002. Mechanisms of thermohaline mode switching with application to warm equable climates. J. Climate 15, 2056–2072. https://doi.org/10.1175/1520-0442(2002)015,2056:MOTMSW.2.0.CO;2.

Zhang, R., Sutton, R., Danabasoglu, G., et al., 2019. A review of the role of the Atlantic Meridional Overturning Circulation in Atlantic multidecadal variability and associated climate impacts. Rev. Geophys. 57 (2), 316–375. https://doi.org/10.1029/2019RG000644.